Bimetallic oxidative addition in nickel-catalyzed alkyl-aryl Kumada coupling reactions

Jan Breitenfeld,[1] Matthew D. Wodrich,[2] and Xile Hu*[1]

[1] Laboratory of Inorganic Synthesis and Catalysis, [2] Laboratory of Computational Molecular Design, Institute of Chemical Sciences and Engineering, École Polytechnique Fédérale de Lausanne (EPFL), EPFL-ISIC-LSCI, BCH 3305, Lausanne, CH 1015, Switzerland.

E-mail: xile.hu@epfl.ch

TOC graphic

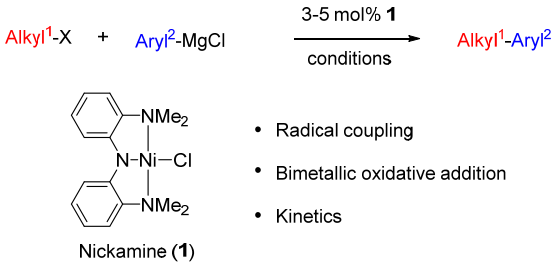

Abstract

The mechanism of alkyl-aryl Kumada coupling catalyzed by the nickel pincer complex Nickamine was studied. Experiments using radical-probe substrates and DFT calculations established a bimetallic oxidative addition mechanism. Kinetic measurements showed that transmetalation rather than oxidative addition was the turnover determining step. The transmetalation involved a bimetallic pathway.

1. Introduction

In recent years, significant progress has been made in nickel-catalyzed cross-coupling of alkyl halides with organometallic nucleophiles.[1-4] However, the mechanistic understanding of these reactions is still limited. There is ample evidence that most coupling involves alkyl radicals originated from alkyl halides.[3,4] This is consistent with the propensity of Ni to undergo single electron transfer reactions in oxidative addition of carbon electrophiles, documented in the classical organometallic literature.[5] For example, Hegedus proposed in 1975 that reactions of the isolated Ni(II) π-allyl Br complex with alkyl halide produced first alkyl radical,[6] although he later revised the mechanism of this reaction to a SN_2 process.[7] Kochi showed in 1979 that oxidative addition of aryl halides on Ni(0) proceeded via a first single electron transfer.[8] On the other hand, the mechanism beyond the radical initiation step for the newly developed coupling reactions is largely speculative. Moreover, the actual catalysts in most systems are unidentified. By studying the reactivity of isolated Ni-terpyridine complexes, Vicic showed that for alkyl-alkyl Negishi coupling reactions catalyzed by the Ni-terpyridine combination, Ni(I) terpyridine alkyl complex rather than analogous Ni(II) species was the active species to react with alkyl halides.[9-11] Our group has developed a nickel(II) pincer complex [($^{Me}N_2N$)Ni-Cl] (**1**, Nickamine)[12] as a catalyst for the coupling of unactivated alkyl halides with alkyl, aryl, and alkynyl Grignard reagents (Figure 1).[13-17] The well-defined nature of Nickamine prompted us to study the mechanism of these Kumada coupling reactions.[18,19] Recently, such study led to the discovery of a bimetallic radical oxidative addition mechanism for Ni-catalyzed alkyl-alkyl Kumada coupling.[20] In this mechanism, two nickel(II) alkyl species are involved in the oxidative addition of the alkyl halide, making the highest formal oxidation state of nickel during catalysis +3. The study provided a rare example where the reaction pathways after the generation of alkyl radicals in Ni-catalyzed coupling of alkyl halides were thoroughly probed by experimental and computational methods. While the study was specific to the reactions catalyzed by **1**, the groups of Weix, Mirica, and Tilley subsequently showed evidence for organometallic Ni(III) intermediates and the involvement of two Ni(III) species in related C-C coupling reactions.[21-23]

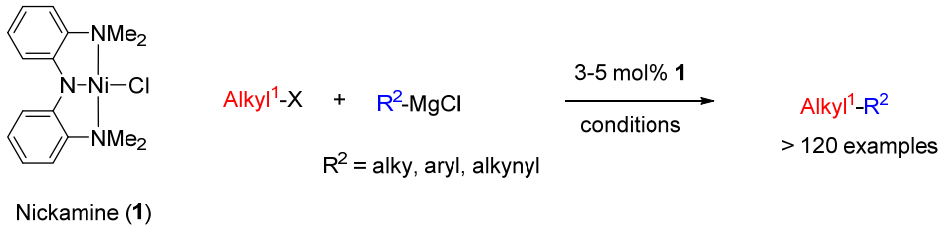

Figure 1. Nickamine and the Kumada coupling reactions catalyzed by Nickamine.

The Nickamine catalyst is versatile. In addition to alkyl-alkyl Kumada coupling, it also catalyzes alkyl-aryl and alkyl-alkynyl Kumada coupling as well as alkyl-alkyl and alkyl-aryl Suzuki coupling.[24] To deduce a general trend in the catalysis by Nickamine and to enhance the understanding of Ni-catalysis, we studied several mechanistic features of the alkyl-aryl Kumada coupling which are described here.

2. Results

2.1 Radical Coupling

We previously reported evidence that the activation of alkyl halides produces alkyl radical intermediates in the alkyl-aryl coupling catalyzed by **1**. For example, when (bromomethyl)cyclopropane was coupled to PhMgCl, the ring-opened product 4-phenyl-1-butene was isolated as the main product.[15] This result is consistent with the formation of cyclopropyl methyl radical which undergoes rapid ring-opening rearrangement. When 3 and 4-methyl cyclohexyl iodides were coupled to PhMgCl, a constant and high diastereoselectivity was obtained regardless of the initial ratios of the cis and trans-isomers.[17] This outcome can only be explained by the formation of substituted cyclohexyl radicals.[17]

Based on literature of oxidative addition involving radicals,[5] three possible pathways can be proposed for the coupling: cage-rebound, escape-rebound, and bimetallic oxidative addition (Scheme 1). Kochi proposed a cage-rebound mechanism for the oxidative addition of aryl halide on Ni(0);[8] Finke showed that a Co(III) alkyl Coenzyme B12 model complex underwent a Co to carbon alkyl bond rearrangement via a free alkyl radical, i.e., escape-rebound rather than cage-rebound pathway because the latter was much slower;[25] and finally, oxidative addition on two metals was well known for 17 electron transition metal complexes.[5,26] As reported before, the Ni(II) halide complex **1** is inactive towards alkyl halide,[12] while certain Ni(II) aryl species is active.[15] In the cage-rebound pathway (Path A), an organometallic Ni(II)

aryl species activates alkyl halide to generate an alkyl radical and a formal Ni(III) halide spcies (although this Ni(III) species might be a Ni(II)-ligand cation complex). Recombination of the alkyl radical with the Ni(III) species in the cage gives a formal Ni(IV) species which reductively eliminates the coupling product and regenerates a Ni(II) halide complex. The escape-rebound pathway (Path B) is different from the cage-rebound pathway in that the alkyl radical first escapes and then reenters the solvent cage to recombine with the formal Ni(III) halide complex to give the formal Ni(IV) species. In the bimetallic oxidative addition pathway (Path C), the alkyl radical escapes the solvent cage and recombines with a second molecule of Ni(II) aryl species to form a formal Ni(III) aryl alkyl species which reductively eliminates the coupling product and gives a Ni(I) species. C-C reductive elimination from Ni(III) intermediates were commonly proposed in Ni-mediated or catalyzed C-C bond forming reactions. Kochi provided evidence for such a reaction in 1975[27] and Mirica recently observed C-C reductive elimination from a Ni(III) aryl alkyl complex.[22] The Ni(I) species recombines with the formal Ni(III) halide complex to give two Ni(II) species which can reenter the catalytic cycle. The three proposed reaction pathways take no account of possible homolytic Ni-alkyl bond hemolysis and its influence in the outcome of the reactions.[26] This is reasonable because the homolysis is calculated to have significant kinetic barriers (see below).

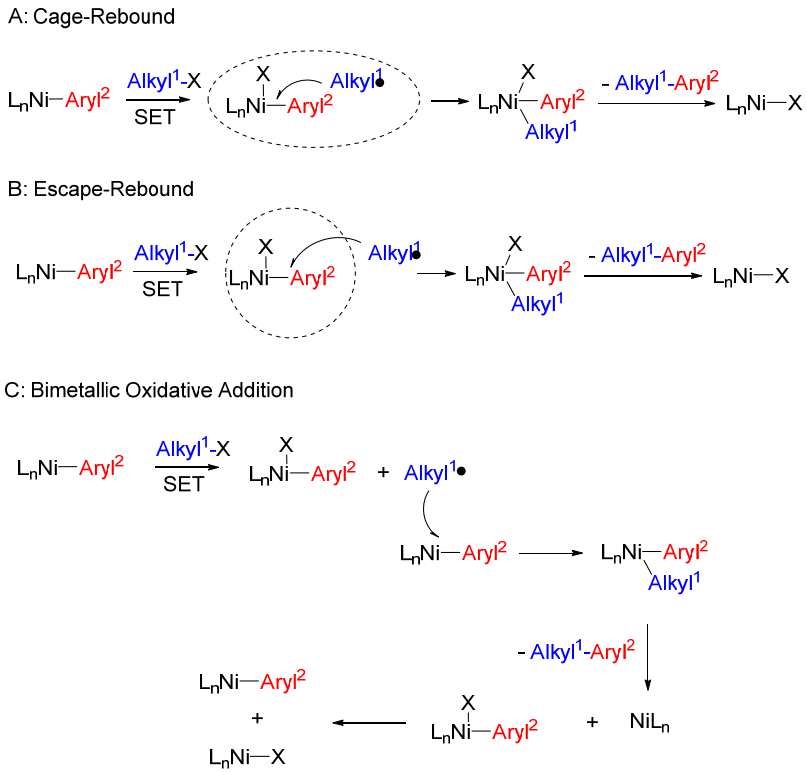

Scheme 1. There pathways for the alkyl-aryl coupling.

The three reaction pathways might be differentiated by the results of cross coupling of radical-probe substrates.[20,28,29] For the alkyl-alkyl coupling catalyzed by **1**, 3-(2-bromoethoxy)prop-1-ene (**2**) is a suitable substrate.[20] Radical activation of **2** during catalysis gives radical **3,** which is subject to a fast intramolecular rearrangement to give the cyclized radical **4**. The ensuing coupling steps then transform **3** and **4** into the linear product **5** and the cyclized product **6** (Scheme 2). The dependence of the ratio of **5** to **6** on the catalyst concentration can be used to differentiate the reaction pathways in Scheme 1. The cage-rebound reaction is an intramolecular reaction and thus, it is zero order on the catalyst. The escape-rebound and bimetallic oxidative addition reactions, on the other hand, are intermolecular and should be first order with respect to catalyst. Therefore, the ratio of **5** to **6** should be independent to catalyst concentration if the cage-rebound pathway occurs, or be first-order in catalyst concentration if the escape-rebound or bimetallic oxidative addition pathway occurs. For the coupling of **2** with ^{n}BuMgCl, a first order dependence of the ratio of the linear to cyclized product was observed, which ruled out the cage-rebound pathway.

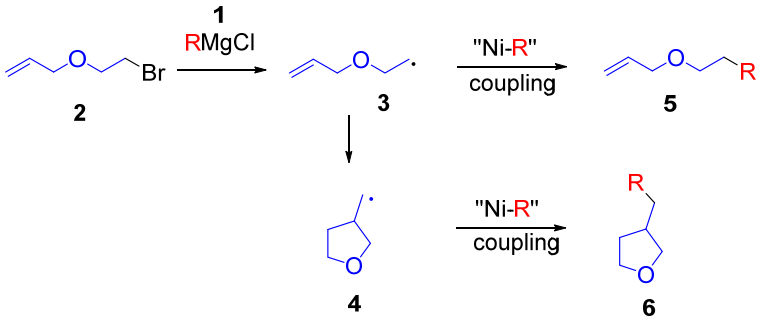

Scheme 2. Coupling reaction of substrate **2** as a mechanistic probe.

To extend the above study to the alkyl-aryl coupling by catalyst **1**, the coupling of **2** with PhMgCl was conducted. However, only the cyclized product, 3-benzyltetrahydrofuran, was obtained under various loading of catalyst (Scheme 3). It appeared that the rearrangement of alkyl radical **3** in the alkyl-aryl coupling was too fast to enable the formation of both the linear and cyclized products.

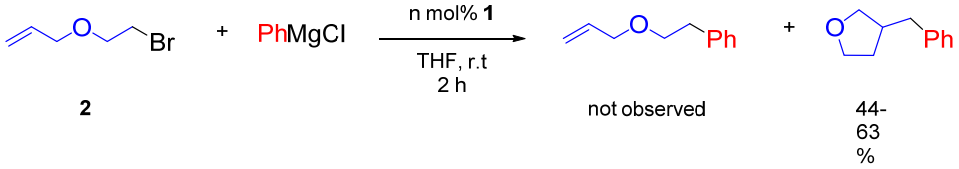

Scheme 3. Coupling of **2** with PhMgCl**.**

Consequently, 6-bromo-1-hexene (**7**) was chosen as the radical-probe. Alkyl radical produced from **7** have an intramolecular rearrangement rate constant of 10^5 s^{-1}.[30,31] Indeed, both the linear (**8**) and the cyclized (**9**) coupling products were observed in the coupling of **7** with PhMgCl. The dependence of the ratio of **8** to **9** on the catalyst loading was then determined. The ratio is first order in catalyst loading (Figure 2). Therefore, the alkyl-aryl coupling follows either the bimetallic oxidative addition or the escape-rebound pathway. The cage-rebound pathway is excluded.

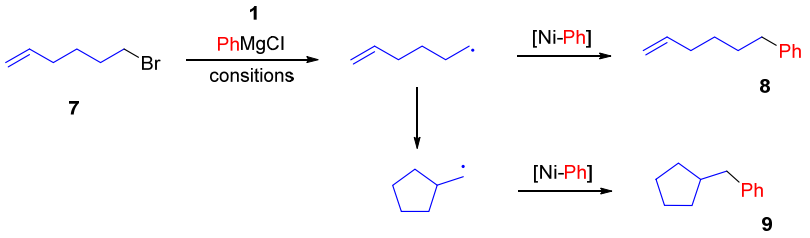

Scheme 4. Coupling of **7** with PhMgCl.

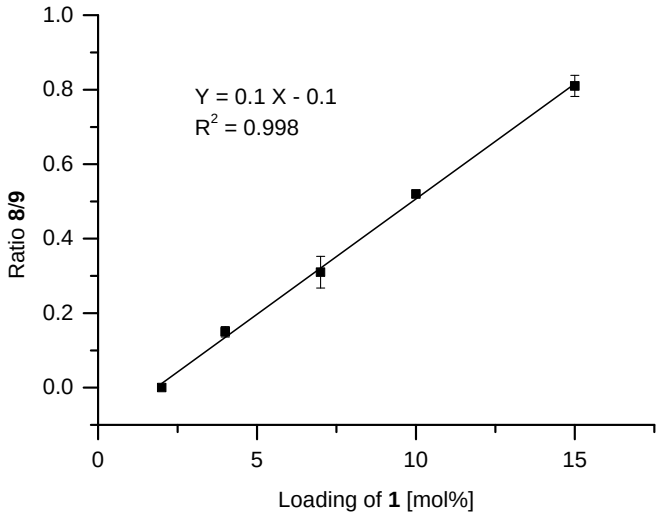

Figure 2. Ratios of the linear and cyclized coupling products **8** and **9** and their dependence on the catalyst loading. At each loading, three independent trials were conducted to obtain an averaged ratio.

To provide additional insight into the cross-coupling mechanism density functional theory computations were undertaken. All structures were first optimized in Gaussian09[32] using the def2-SVP basis set[33] in tandem with Truhlar's M06 functional[34,35] which accurately describes organometallic species. Refined energy estimates were then obtained from single point computations on the M06 geometries using the PBE0[36,37] functional appended with a density dependent dispersion correction (-dDsC)[38-41] to improve the energetic description of long-range non-bonded interactions. PBE0-dDsC computations used the TZ2P slater-type orbital basis set in ADF.[42,43] Solvation corrections, also computed at the PBE0-dDsC/TZ2P//M06/def2-SVP level, were determined in THF solvent using Klamt's Continuum Solvation Model for Realistic Solvents[44] (COSMO-RS), also computed in ADF. Reported free energies include unscaled free energy contributions from the M06/def2-SVP computations.

Both the bimetallic oxidative addition and escape-rebound pathways were examined to assess the energetic viability of each mechanism. The starting point for the bimetallic oxidative addition pathway, **B1** (Figure 3), is a closed-shell singlet Ni(II) aryl species. Upon addition of an alkyl radical, a doublet Ni(III) alkyl/aryl species (**B2**) is formed in which the alkyl ligand is located *trans* to the central nitrogen atom of the pincer ligand. An alternative conformation where the aryl ligand is located in the *trans* position is not a stable point on the potential energy surface. Alkyl radical addition to **B1** is an exergonic process that is not associated with a transition state (TS) barrier, as evidenced not only by the overall exergonicity of the reaction free energy (**B1**+Pr•→**B2**, Figure 4), but also by constrained potential energy surface scans in which the Pr• is dissociated from **B2** to recreate the reactant species (see below). Defining a precise energetic value, however, is quite difficult, as tasks such as describing the energetics associated with bringing separated solvated species (e.g., **B1** and Pr•) together to form a single complex (**B2**) is best accomplished through molecular dynamic simulations. The main concern regarding the magnitude of the reaction free energy is the ability of **B2** to dissociate the alkyl radical and reform the reactants (**B2**→**B1**+Pr•) rather than undergo reductive elimination proceeding to the observed products (**B2**→$\mathbf{TS_{B2,B3}}$→**B3**). To examine the likelihood of this situation, the energy required to dissociate a propyl radical from the Ni complex was determined via a constrained geometry optimization procedure in which the Ni---C• distance was progressively increased. Energy evaluations at a distance of up to 4.0Å revealed dissociation of the propyl radical requires a minimum of 27 kcal/mol (see SI Figure S9 for details) and that no stationary point on the potential energy surface associated with a van der Waals complex could be located (consistent with spontaneous formation of **B2** from **B1** and Pr•). This energetic picture precludes the notion that dissociation of the alkyl radical and reformation of the reactants is more likely than reductive elimination (associated with a barrier of only 3.4 kcal/mol) and eventual product formation. Once the doublet **B2** species is formed, reductive elimination leading to the alkyl-aryl coupled product proceeds after overcoming a small TS barrier ($\mathbf{TS_{B2,B3}}$) of 3.4 kcal/mol. The newly formed alkyl-aryl and doublet Ni(I) products (**B3**) are significantly stabilized with an overall reaction exergonicity of ~23 kcal/mol (Figure 4).

The alternative escape-rebound pathway commences with structure **E1**, which, based analysis of the computed spin density is a doublet Ni(III) halide (Br) complex

and not a Ni(II) ligand cation complex[45,46] owing to majority of the spin density being located on the nickel center (see SI Figure S10 for details). Addition of the alkyl radical to **E1** requires surmounting a TS barrier of 22.1 kcal/mol (open-shell singlet $\mathbf{TS_{E1,E2}}$, Figure 4) corresponding to approach of the alkyl radical. The resulting singlet **E2** structure, in which the akyl and aryl ligands are located in a *cis* orientation and the aryl ligand is *trans* to the central nitrogen atom of the pincer ligand, was found to be the most energetically favorable conformation. From **E2**, reductive elimination forms the alkyl-aryl product and a singlet Ni(II) bromide complex (**E3**) requiring an additional ~5.5 kcal/mol of energy to overcome the $\mathbf{TS_{E2,E3}}$ barrier. The resulting products are significantly stabilized relative to the reactant compounds (Figure 4).

Based on these findings, the bimetallic oxidative addition pathway is strongly preferred over the escape-rebound pathway based on its superior energetic profile (notably the barrierless association of the alkyl radical and small TS associated with reductive elimination of the alkyl-aryl product). In principle, these two pathways are interconnected by a reaction in which **B1** abstracts a bromine atom from $CH_3CH_2CH_2Br$, forming **E1** and the corresponding propyl radical. However, this process is associated with an endergonic free energy of +26.5 kcal/mol, demonstrating that a move from the bimetallic oxidative addition to the escape-rebound potential energy surfaces is unlikely. The high energy of this process is also in agreement with that previous finding that [($^{Me}N_2N$)Ni-Ph)] is unreactive towards alkyl halide.

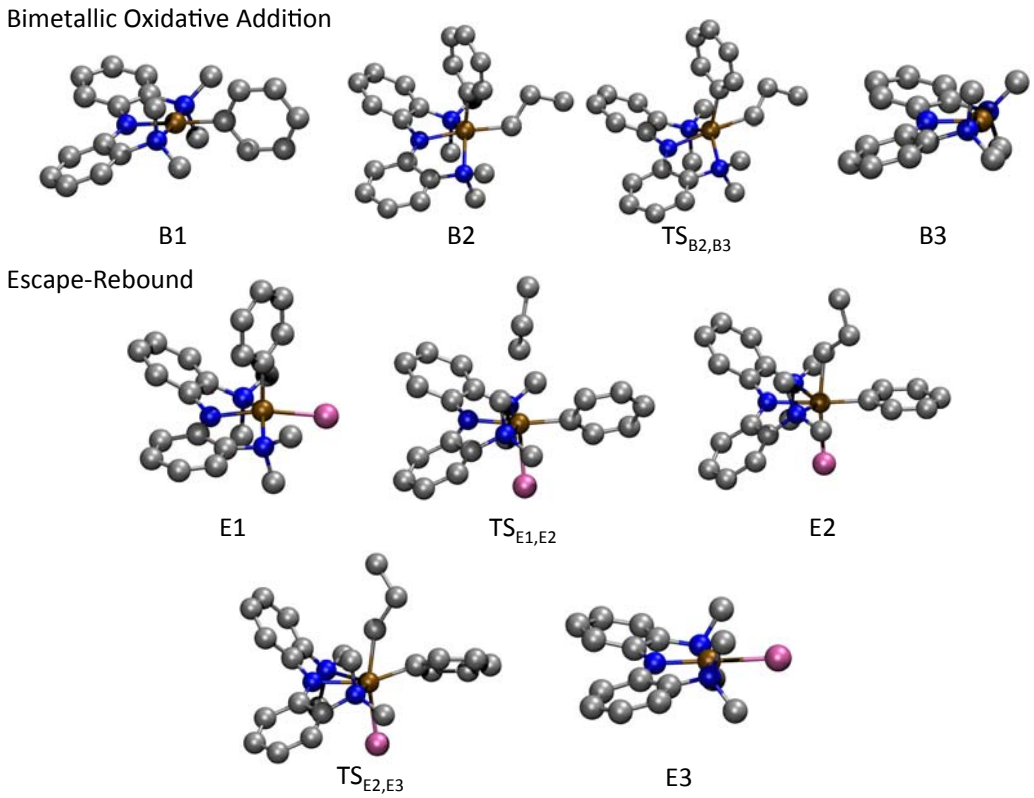

Figure 3. Structures (optimized at the M06/def2-SVP level) of relevant species for the bimetallic oxidative addition and escape-rebound pathways. Atomic color code: carbon=gray, nitrogen=blue, nickel=brown, bromine=purple

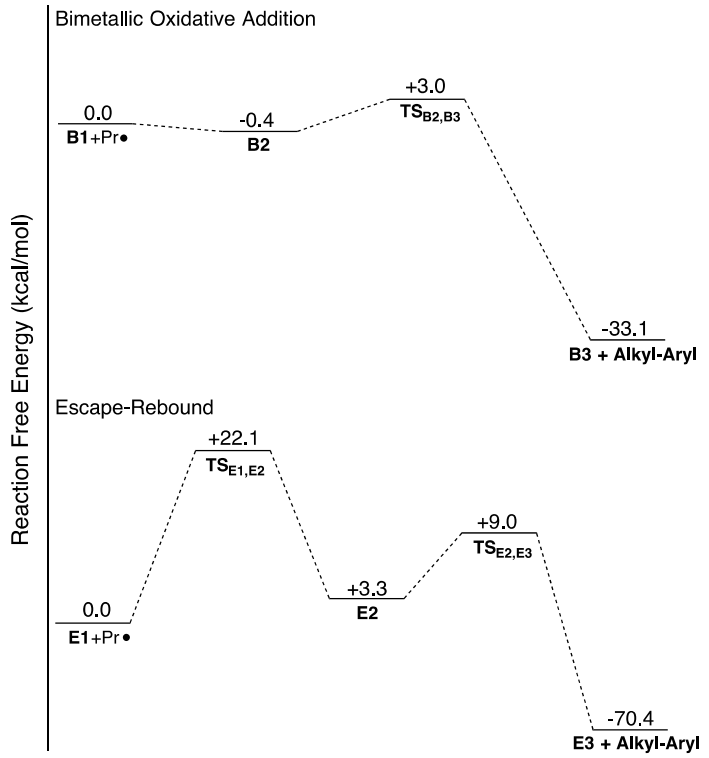

Figure 4. Reaction free energies (in kcal/mol) computed at the PBE0-dDsC/TZ2P//M06/def2-SVP level (in THF solvent using the COMSO-RS solvation model) for the bimetallic oxidative addition and escape-rebound pathways.

2.2 Kinetics

The kinetics of the alkyl-aryl coupling catalyzed by **1** was measured. The coupling of octyl iodide with PhMgCl was chosen as the test reaction (eq 1).

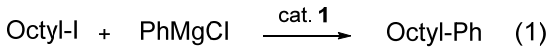

The kinetic measurement necessitated a fast and at-once addition of the Grignard reagent. This was detrimental to the catalysis, which decomposed quickly. In our earlier protocol, a slow addition of Grignard was applied to circumvent this problem. For the kinetics study, this modification is unsuitable. Instead, the temperature of the reaction was decreased from room temperature to 0 ^{o}C where the catalyst was stable even with the fast addition of the Grignard reagent. The initial rate approximation was applied to obtain the reaction rates. Figures 5-7 show that the catalysis is about 2nd-order in catalyst, 2nd order in Grignard reagent, and 0th order in alkyl iodide.

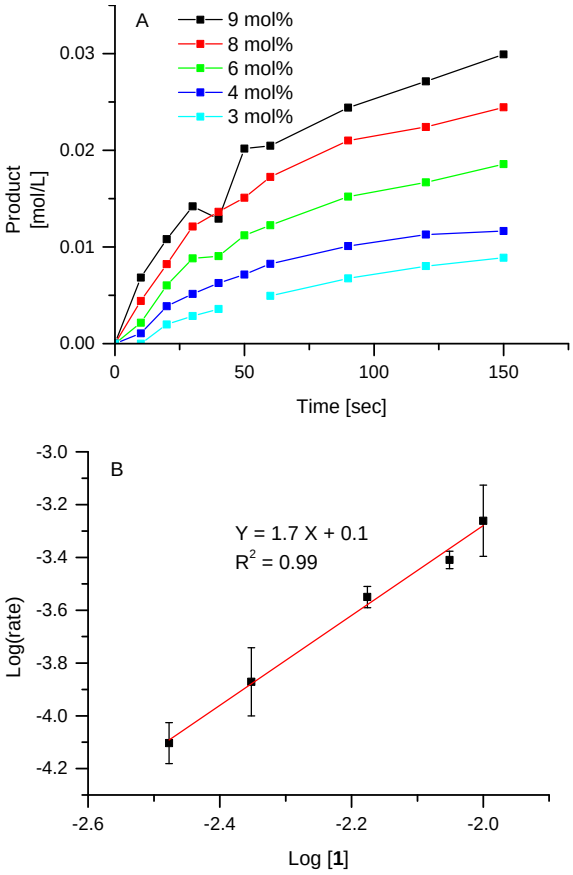

Figure 5. (A) Time-dependent product (octyl-Ph) formation at different catalyst loadings. (B) The plot of log (rate) vs. log([**1**]). The slope is the rate order; the error bars represent the range of results in individual runs.

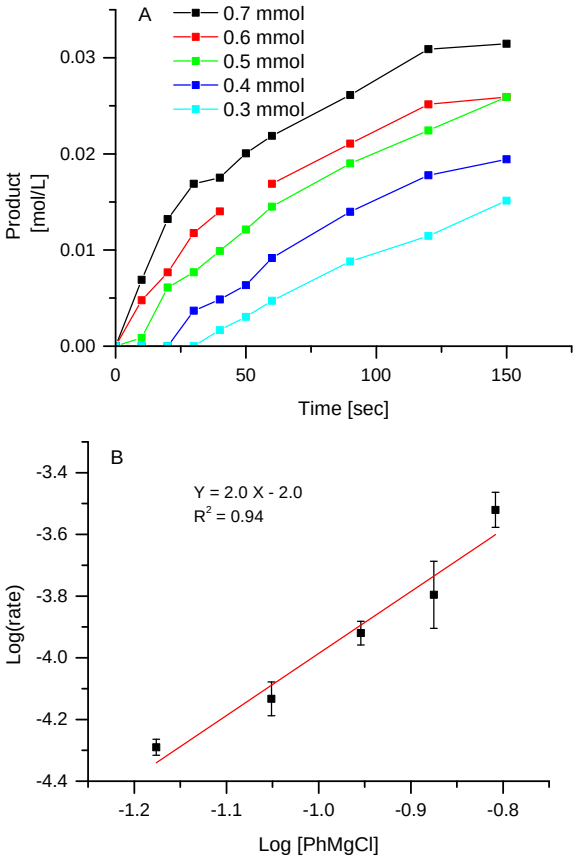

Figure 6. (A) Time-dependent product (octyl-Ph) formation at different loadings of PhMgCl. (B) The plot of log (rate) vs. log([PhMgCl]). The slope is the rate order; the error bars represent the range of results in individual runs..

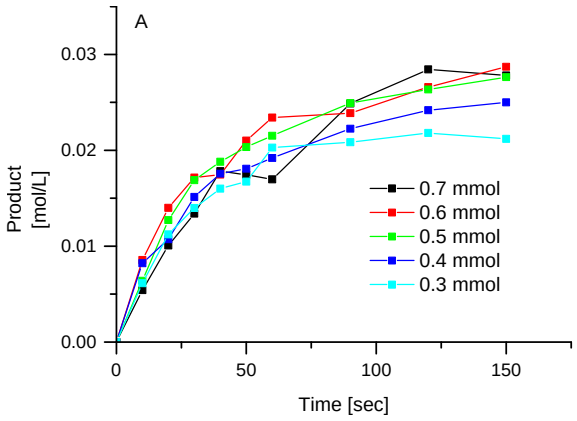

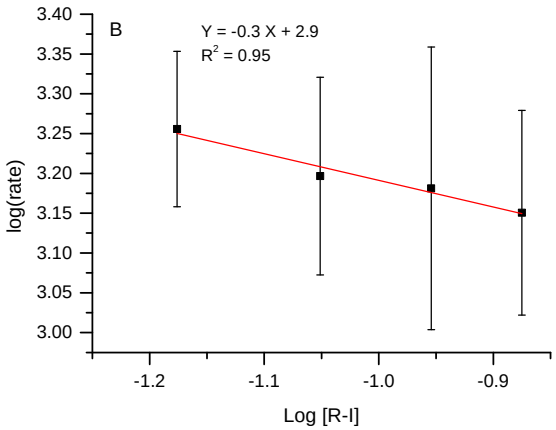

Figure 7. (A) Time-dependent product (octyl-Ph) formation at different loadings of octyl-I. (B) The plot of log (rate) vs. log([Octyl-I]). The slope is the rate order; the error bars represent the range of results in individual runs.

3. Discussion

The mechanistic study presented here favors a bimetallic oxidative addition pathway for the alkyl-aryl coupling catalyzed by Nickamine. This pathway is similar to the reaction pathway of the alkyl-alkyl coupling catalyzed by the same catalyst.[20] The combination of an alkyl radical with a Ni aryl species is slower than analogous reaction with a Ni alkyl species. The former is compatible with a radical clock having a rearrangement rate constant of 10^{-5} s^{-1}, whereas the latter is compatible with a radical clock having a rearrangement rate constant of 10^{-6} s^{-1}. Homolysis of Ni-alkyl bonds might complicate the comparison of recombination rates using radical probes; however, as shown in Figure 4, homolysis is unfavorable for the Ni(IIII) alkyl intermediates.

Previously we reported evidence that defined N_2N-Ni complexes rather than their decomposed forms such as Ni nanoparticles or nickelates were the actual catalysts for the alkyl-aryl Kumada coupling. The evidence includes the identification of [($^{Me}N_2N$)Ni-Ph)] as the resting state of catalyst, the nearly quantitative isolation of [($^{Me}N_2N$)Ni-Ph)] in the end of catalysis, and the negative Hg-poisoning test.[15] It was also shown that [($^{Me}N_2N$)Ni-Ph)] did not react with alkyl halide; rather, this complex needed to be activated by PhMgCl before reacting with alkyl halide.[15] An unstable species [($^{Me}N_2N$)Ni-Ph)](PhMgCl) was proposed as the active species. Similar observation was made in the alkyl-alkyl Kumada coupling, where an analogous

[($^{Me}N_2N$)Ni-alkyl)](alkyl-MgCl) species was responsible for the activation of alkyl halide during catalysis.[20] This is another common feature between the two coupling reactions.

The 0th order in alkyl halide indicates that the turnover-determining step is not oxidative addition. The 2nd order in both catalyst and Grignard reagent suggests that an unusual transmetalation step is turnover determining. The 2nd order in catalyst was previously reported by Yamamoto and co-workers in Ni(0)-promoted biaryl coupling of aryl bromide.[47,48] The rate-determining step was the "redistributive " transmetalation of two Ni(L)(Ph)(Br) molecules to form Ni(L)(Ph)$_2$ and Ni(L)(Br)$_2$ (eq. 2). Reductive elimination from Ni(L)(Ph)$_2$ gave the biphenyl product.

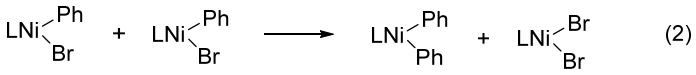

(2)

As [($^{Me}N_2N$)Ni-Ar)](ArMgCl) (**10**) is the active species, its formation is proposed as the turnover determining step. To account for 2nd order in both catalyst and Griganrd reagent, the following transmetalation sequence is proposed: in a pre-equilibrium, [($^{Me}N_2N$)Ni-X)] (X = halide) (**11**) forms an unstable adduct with ArMgCl to give [($^{Me}N_2N$)Ni-X)](ArMgCl) (**12**). Two molecules of **12** then undergo a "redistribution " to give **10**, **11**, and MgClX (eq. 3). If the redistribution is the turnover-determining step, then the observed kinetics can be explained. Evidence for the association of [($^{Me}N_2N$)Ni-X)] with alkyl Grignard reagent was reported;[20] this association might be attributed to the interaction between the Lewis basic ligand and the Lewis acidic Mg cation.

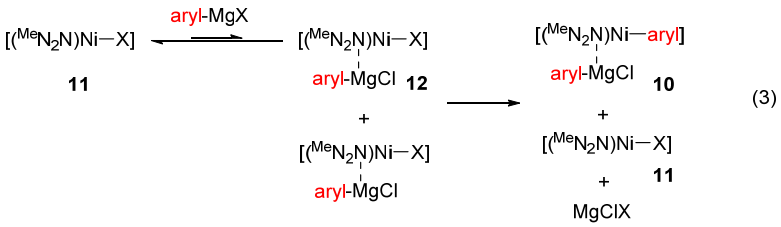

(3)

A complete catalytic cycle for for the alkyl-aryl Kumada coupling catalyzed by Nickamine can be now proposed (Figure 8). The nickel(II) halide complex (**11**) is transmetalated in a bimetallic and proportionative manner to give the key intermediate [($^{Me}N_2N$)Ni-Ar](ArMgCl) (**10**) which is in equilibrium with the dormant species [($^{Me}N_2N$)Ni-Ar] (**13**). Intermediate **10** activates the alkyl halide to give a one-electron

oxidized complex [(^{Me}N$_2$N)Ni(X)(Ar)] (**14**) and the alkyl radical. The associated ArMgCl in **10** may have dissociated at this point. The alkyl radical then reacts with a second molecule of [(^{Me}N$_2$N)Ni-Ar](Ar-MgCl) or [(^{Me}N$_2$N)Ni-Ar] to yield [(^{Me}N$_2$N)Ni(Ar)(alkyl)] (**15**). Reductive elimination from **15** gives the alkyl-aryl coupling product and a nickel(I) species [(^{Me}N$_2$N)Ni] (**16**). Comproportionation of **16** with the initially formed nickel(III) species **14** regenerates [(^{Me}N$_2$N)Ni-X] (**11**) and [(^{Me}N$_2$N)Ni-Ar] (**13**), both of which can re-enter the catalytic cycle.

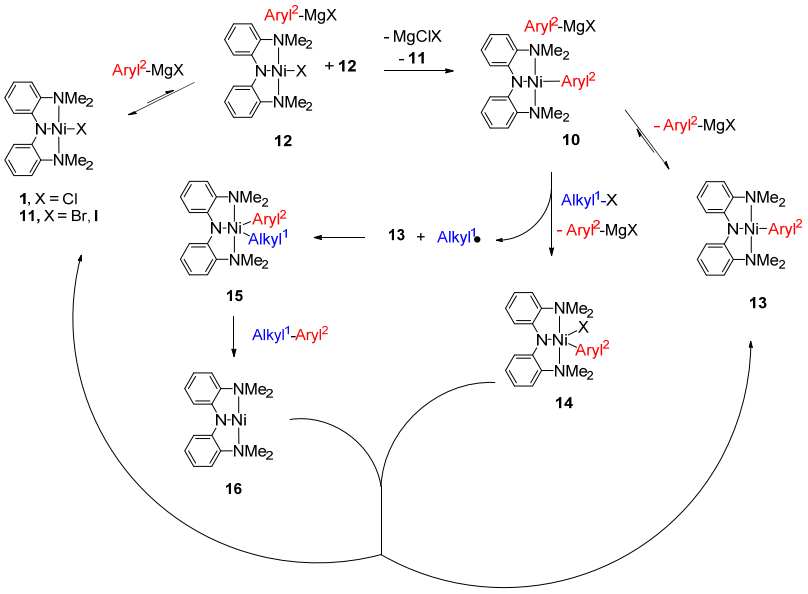

Figure 8. The proposed catalytic cycle for alkyl-aryl Kumada coupling catalyzed by Nickamine.

4. Conclusion

The mechanism of alkyl-aryl Kumada coupling reactions catalyzed by Nickamine was investigated. Reactions using a radical-probe substrate and DFT computations established a bimetallic oxidative addition pathway for the radical activation of alkyl halide and the subsequent C-C bond formation. In this pathway, two Ni(II) aryl species are required to supply the two electrons to alkyl halide. The highest formal oxidation state of Ni-containing intermediate is +3. The kinetics of the catalysis was measured to reveal transmetalation rather than oxidative addition as the turnover-determining step. The product of transmetalation is the doubly arylated species [(^{Me}N$_2$N)Ni-Ar](ArMgCl). The mechanism of the alkyl-aryl coupling is analogous to the mechanism of alkyl-alkyl coupling, indicating a unifying reaction pathway in the coupling of alkyl halides using Nickamine as catalyst.

Experimental

Chemicals and Reagents

All manipulations were carried out under a N_2 atmosphere using standard Schlenk or glovebox techniques. Solvent was purified using a two-column solid-state purification system (Innovative Technology, NJ, USA) and transferred to the glove box without exposure to air by the aid of a Straus flask. Deuterated solvents were purchased from Cambridge Isotope Laboratories, Inc., and stored over activated 3 Å molecular sieves, after degassing by Freeze-Pump-Thaw method. TMEDA (*N*,*N*,*N*′,*N*′-Tetramethylethylenediamine), phenyl magnesium chloride (PhMgCl), octyl iodide, 6-bromo-1-hexene, and decane were purchased from Sigma Aldrich and were used without further purification. Complex [($^{Me}NN_2$)NiCl] (**1**) was prepared according to the literature.[12,49]

Physical methods

^1H and $^{13}C\{^1H\}$ NMR spectra were recorded at an ambient temperature on a Bruker Avance 400 spectrometer. ^1H NMR and $^{13}C\{^1H\}$ chemical shifts were referenced to residual solvent as determined relative to TMS (δ = 0.00 ppm). GC measurement was conducted on a Perkin-Elmer Clarus 400 GC with a FID detector. GC-MS measurements were conducted on a Perkin-Elmer Clarus 600 GC equipped with Clarus 600T MS and a FID detector.

Coupling of PhMgCl with 6-bromo-1-hexene:

Typically, five reactions (five different concentrations of **1**) were run simultaneously in order to maintain identical reaction conditions and to assure the quality of the data. Prior to the experiments, the following solutions were prepared and the concentration of PhMgCl (2 M) was verified by a literature method prior to use:[50]

(*A*) A solution of [(N_2N)Ni-Cl] (69.7 mg, 0.2 mmol, 0.2 M) in 1 mL THF was used to prepare five solutions, each with a total volume of 0.5 mL THF and a loading of **1** of 0.01 mmol (2 mol%), 0.02 mmol (4 mol%), 0.035 mmol (7 mol%), 0.5 mmol (10 mol%), or 0.075 mmol (15 mol%).

(*B*) A solution of 6-bromo-1-hexene (407.5 mg, 2.5 mmol, 1 M) and $C_{12}H_{26}$ (255 mg, 1.5 mmol, 0.3 M) in 5 mL THF.

(*C*) A solution of TMEDA (407.5 mg, 2.5 mmol, 1 M) in 2.5 mL THF.
Inside the glovebox, five vials were charged with one of the previously prepared solutions of *A* (containing 15 mol% - 2 mol% of **1**), 1 mL of solution *B* (0.5 mmol octyl iodide plus 0.3 mmol $C_{12}H_{26}$). Then, 0.5 mL PhMgCl (2 M in THF, 0.5 mmol) and 0.5 mL of solution *C* (0.3 mmol TMEDA) were combined and added slowly (~1h) to each vial by syringe pump under stirring. After the addition was complete, the solution was stirred for another 60 minutes. The reaction was quenched with water (5 mL), extracted with diethyl ether (2 x 10 mL), dried over Na_2SO_4 and filtered. A GC vial was charged with 1 mL of the respective reaction mixture and analyzed. The yields, the conversions, and the ratios of products were obtained by GC-MS using $C_{12}H_{26}$ as internal standard (the FID detector was used for the quantification).

The linear (**8**) and cyclic (**9**) products were isolated using the following conditions: the solvent of the extracted solution after the catalysis was removed by rotary evaporation. After purification by preparative TLC using hexane/ethyl acetate (10/1), **8** and **9** were isolated as oils. The spectral properties of **8** and **9** match those reported in literature.
NMR data for **9**:[24]
^{1}H NMR (400 MHz, $CDCl_3$): δ = 7.28 (d, J = 9.3 Hz, 2 H), 7.24–7.01 (m, 3 H), 2.62 (d, J = 7.3 Hz, 2 H), 2.22–1.94 (m, 1 H), 1.68 (dd, J = 21.0, 8.5 Hz, 4 H), 1.55 (d, J = 11.9 Hz, 2 H), 1.41–1.07 (m, 2 H). ^{13}C{^{1}H} NMR (100 MHz, $CDCl_3$): δ = 142.5, 128.9, 128.3, 125.7, 42.3, 42.2, 32.6, 25.1.

NMR data for for **8**:[51]
^{1}H NMR (400 MHz, $CDCl_3$) δ 7.48 – 7.05 (m, 1H), 5.83 (ddd, *J* = 17.0, 6.7, 3.5 Hz, 1H), 4.98 (ddd, *J* = 13.9, 10.2, 9.1 Hz, 1H), 2.64 (t, *J* = 7.7 Hz, 1H), 2.11 (dd, *J* = 14.4, 7.0 Hz, 1H), 1.78 – 1.56 (m, 1H), 1.46 (t, *J* = 7.6 Hz, 1H).
^{13}C NMR (100 MHz, $CDCl_3$) δ 142.82, 139.00, 128.53, 128.37, 125.74, 114.52, 35.94, 33.78, 31.10, 28.68.

Coupling of PhMgCl with 3-(2-bromoethoxy)prop-1-ene:

A similar procedure as the coupling with 6-bromo-1-hexene was applied, expect that the solution *B* was modified accordingly:

(*B*) A solution of 3-(2-bromoethoxy)prop-1-ene (407.5 mg, 2.5 mmol, 1 M) and $C_{12}H_{26}$ (255 mg, 1.5 mmol, 0.3 M) in 5 mL THF.
The workup was identical to those of **8** and **9**. The product 3-benzyltetrahydrofuran was isolated as a colorless oil. NMR data of 3-benzyltetrahydrofuran match those of the literature.[52,53]

^{1}H NMR (400 MHz, $CDCl_3$) δ 7.42 – 7.09 (m, 5H), 4.03 – 3.65 (m, 3H), 3.45 (dd, J = 8.3, 6.7 Hz, 1H), 2.79 – 2.59 (m, 2H), 2.50 (dd, J = 14.5, 7.3 Hz, 1H), 2.06 – 1.87 (m, 1H), 1.71 – 1.51 (m, 1H). ^{13}C NMR (101 MHz, $CDCl_3$) δ 140.81, 128.68, 128.43, 126.07, 77.48, 77.16, 76.84, 73.00, 67.87, 40.99, 39.35, 32.18.

Kinetic study - dependence on PhMgCl

Remark: Under standard catalytic conditions the Grignard reagent is added slowly by a syringe pump. If Grignard is added fast in one portion, decomposition of the catalyst was observed. Therefore, the reaction was cooled to avoid decomposition as a fast, at once addition of Grignard reagent was required. In a typical experiment, five reactions (five different concentrations of PhMgCl) were run consecutively in order to maintain identical reaction conditions and assure the quality of the data. Prior to the experiments, the following standard solutions were prepared:
(A) [(N_2N)Ni- Cl] (87.0 mg, 0.25 mmol, 0.05 M) in 5 mL THF;
(B) Octyl iodide (482 mg, 2.50 mmol, 0.25 M) with $C_{12}H_{26}$ (255 mg, 2.50 mmol, 0.25 M) and TMEDA (290 mg, 1.50 mmol, 0.25 M) in 10 mL THF
(C) PhMgCl (1 M, 5 mL THF); the concentration of PhMgCl was verified checked by a literature method prior to use.[50]
Then five solutions with a total volume of 1.5 mL each were prepared containing 0.70 mmol, 0.60 mmol, 0.50 mmol, 0.40 mmol, and 0.3 mmol of PhMgCl (THF was used to dilute), respectively.
Inside the glovebox, five vials with new rubber septum were charged with 0.5 mL of solution *A* (0.05 mmol, 5mol% of **1**), 2.0 mL of solution *B* (0.50 mmol octyl iodide plus 0.50 mmol TMEDA plus 0.30 mmol $C_{12}H_{26}$) and 0.5 mL THF. The vials were transferred outside the glovebox and the following procedure applied to one after the other: One vial was placed inside a cooling bath at –0°C (ice/water) under a N_2 atmosphere (pierced by needle) for 3 min under stirring. The septum was removed

while N_2 flow was maintained and an aliquot (60 µL) was collected and immediately transferred into a GC vial containing 60 µL of acetonitrile. Then one of the previously prepared PhMgCl solution (*vide supra*) was added quickly under stirring. Every 10 seconds an aliquot (60 µL) was collected and immediately transferred into a GC vial containing acetonitrile (60 µL) to quench the reaction. After 60 seconds, an aliquot (60 µL) was collected every 30 seconds up to 150 seconds and was immediately transferred into a GC vial containing acetonitrile (60 µL). Then 1 mL of Et_2O was added to each GC samples. The yields and the conversions were obtained by GC using $C_{12}H_{26}$ as an internal standard.

The kinetic data were analyzed by the initial rate method, with the assumption that data up to a maximum of 10% yield can be used. The data of the concentration of product vs. time plot was fitted by a linear equation. The obtained slopes represent the reaction rates. The order of Grignard was derived from a linear fit of the log(rate) vs. log([PhMgCl]) plot. Two independent trials were conducted for each experiment.

Kinetic study -dependence on catalyst loading

In a typical experiment, five reactions (five different concentrations of **1** were run consecutively in order to maintain identical reaction conditions and ascertain the quality of the data. Prior to the experiments, the following standard solutions were prepared:

(A) [(N_2N)Ni- Cl] (87.0 mg, 0.25 mmol, 0.05 M) in 5 mL THF. Then five solution with a total volume of 1 mL each were prepared containing 0.045 mmol (9 mol%), 0.04 mmol (8 mol%), 0.03 mmol (6 mol%), 0.02 mmol (4 mol%), and 0.015 mmol (3 mol%) of **1** (THF was used to dilute), respectively.

(B) Octyl iodide (482 mg, 2.5 mmol, 0.25 M) with $C_{12}H_{26}$ (255 mg, 1.5 mmol, 0.3 M), and TMEDA (290 mg, 2.5 mmol, 0.25 M) in 10 mL THF;

(C) PhMgCl (0.4 M, 8 mL THF).

Inside the glovebox, five vials with new rubber septum were charged with one of the previously prepared solutions of *A* (9 mol% - 3 mol% of **1**) and 2 mL of solution *B* (0.5 mmol octyl iodide plus 0.5 mmol TMEDA plus 0.3 mmol $C_{12}H_{26}$). The vials were transferred outside the glovebox and the following procedure applied to one after the other: One vial placed inside a cooling bath at –0°C (ice/water) under a N_2 atmosphere (pierced by needle) for 3 min under stirring. The septum was removed

while N_2 flow was maintained and an aliquot (60 μL) was collected and immediately transferred into a GC vial containing 60 μL of acetonitrile. Then 1.5 mL of solution *C* was added quickly under stirring. Every 10 seconds, an aliquot (60 μL) was collected and immediately transferred into a GC vial containing acetonitrile (60 μL) to quench the reaction. After 60 seconds, an aliquot (60 μL) was collected every 30 seconds up to 150 seconds and was immediately transferred into a GC vial containing acetonitrile (60 μL). Then 1 mL of Et_2O was added to each GC samples. The yields and the conversions were obtained by GC using $C_{12}H_{26}$ as an internal standard.

The kinetic data were analyzed by initial rate method, with the assumption that data up to a maximum of 10% yield can be used. The data of the concentration of product vs. time plot was fitted by a linear equation. The obtained slopes represent the reaction rates. The order of catalyst was derived from a linear fit of the log(rate) vs. log([**1**]) plot. Two independent trials were conducted for each experiment.

Kinetic study - dependence on substrate

In a typical experiment, five reactions (five different concentrations of octyl iodide were run consecutively in order to maintain identical reaction conditions and ascertain the quality of the data. Prior to the experiment the following standard solutions were prepared:

(A) [(N_2N)Ni- Cl] (43.5.0 mg, 0.125 mmol, 0.025 M), $C_{12}H_{26}$ (255 mg, 1.5 mmol, 0.3 M), and TMEDA (290 mg, 2.5 mmol, 0.5 M) in 5 mL THF;

(*B*) Octyl iodide (965 mg, 5.0 mmol, 1 M) in 5 mL THF. Then five solution with a total volume of 1.5 mL each were prepared containing 0.7 mmol, 0.6 mmol, 0.5 mmol, 0.4 mmol, and 0.3 mmol of octyl iodide (THF was used to dilute), respectively.

(C) PhMgCl (0.4 M, 8 mL THF).

Inside the glovebox, five vials with new rubber septums were charged with 0.5 mL of solution *A* (0.01 mmol or 4mol% of **1**), one of the previously prepared solutions *B* (0.25 mmol – 0.050 mmol of 2-bromoethyl)benzene) and 2 mL THF. The vials were transferred outside the glovebox and the following procedure applied to one after the other: One vial placed inside a cooling bath at –0°C (ice/water) under a N_2 atmosphere (pierced by needle) for 3 min with stirring. The septum was removed while N_2 flow was maintained and an aliquot (60 μL) was collected and immediately

transferred into a GC vial containing 60 μL of acetonitrile. Then 1.5 mL of solution *C* was added quickly under stirring. Every 10 seconds, an aliquot (60 μL) was collected and immediately transferred into a GC vial containing acetonitrile (60 μL) to quench the reaction. After 60 seconds, an aliquot (60 μL) was collected every 30 seconds up to 150 seconds and was immediately transferred into a GC vial containing acetonitrile (60 μL). The yields and the conversions were obtained by GC using $C_{10}H_{22}$ as an internal standard.

The kinetic data were analyzed by the initial rate method, with the assumption that data up to a maximum of 10% yield can be used. The data of the concentration of product vs. time plot was fitted by a linear equation. The obtained slopes represent the reaction rates. The order of octyl iodide was derived from a linear fit of the log(rate) vs. log([octyl-I]) plot. Two independent trials were conducted for each experiment.

Computational Details

Geometry optimizations were performed at the M06-2X[29]/def2-SVP[30] level using the "ultrafine" grid in Gaussian09.[31] Single point energy computations on M06-2X/def2-SVP optimized geometries used the PBE0[32] density functional appended with a density dependent dispersion correction,[33] PBE0-dDsC/TZ2P in ADF.[34] Implicit solvation energies (in tetrahydrofuran) were determined using the COSMO-RS[35] solvation model, as implemented in ADF. Free energies reported include the free energy corrections taken from the M06-2X/def2-SVP computation and the solvation energies determined at the PBE0-dDsC/TZ2P level appended to the PBE0-dDsC/TZ2P//M06-2X/def2-SVP electronic energies.

Acknowledgement

This work is supported by the EPFL and the Swiss National Science Foundation (no. 200020_144393/1). MDW thanks Prof. Clémence Corminboeuf (EPFL) for helpful suggestions and comments. The Laboratory for Computational Molecular Design at EPFL is acknowledged for providing computational resources.

Supporting information available: Mass and NMR spectra and computational details. This material is available free of charge via the Internet at http://pubs.acs.org.

Reference

(1) Netherton, M. R.; Fu, G. C. *Adv. Synth. Catal.* **2004**, *346*, 1525-1532.
(2) Terao, J.; Kambe, N. *Acc. Chem. Res.* **2008**, *41*, 1545-1554.
(3) Hu, X. L. *Chem. Sci.* **2011**, *2*, 1867-1886.
(4) Rudolph, A.; Lautens, M. *Angew. Chem., Int. Ed.* **2009**, *48*, 2656-2670.
(5) Hartwig, J. F. *Organotransition Metal Chemistry - From Bonding to Catalysis*; University Science Books: Sausalito, California, 2010.
(6) Hegedus, L. S.; Miller, L. L. *J. Am. Chem. Soc.* **1975**, *97*, 459-460.
(7) Hegedus, L. S.; Thompson, D. H. P. *J. Am. Chem. Soc.* **1985**, *107*, 5663-5669.
(8) Tsou, T. T.; Kochi, J. K. *J. Am. Chem. Soc.* **1979**, *101*, 6319-6332.
(9) Anderson, T. J.; Jones, G. D.; Vicic, D. A. *J. Am. Chem. Soc.* **2004**, *126*, 8100-8101.
(10) Jones, G. D.; Martin, J. L.; McFarland, C.; Allen, O. R.; Hall, R. E.; Haley, A. D.; Brandon, R. J.; Konovalova, T.; Desrochers, P. J.; Pulay, P.; Vicic, D. A. *J. Am. Chem. Soc.* **2006**, *128*, 13175-13183.
(11) Jones, G. D.; McFarland, C.; Anderson, T. J.; Vicic, D. A. *Chem. Commun.* **2005**, 4211-4213.
(12) Csok, Z.; Vechorkin, O.; Harkins, S. B.; Scopelliti, R.; Hu, X. L. *J. Am. Chem. Soc.* **2008**, *130*, 8156-8157.
(13) Vechorkin, O.; Csok, Z.; Scopelliti, R.; Hu, X. L. *Chem.-Eur. J.* **2009**, *15*, 3889-3899.
(14) Vechorkin, O.; Hu, X. L. *Angew. Chem., Int. Ed.* **2009**, *48*, 2937-2940.
(15) Vechorkin, O.; Proust, V.; Hu, X. L. *J. Am. Chem. Soc.* **2009**, *131*, 9756-9766.
(16) Vechorkin, O.; Godinat, A.; Scopelliti, R.; Hu, X. L. *Angew. Chem., Int. Ed.* **2011**, *50*, 11777-11781.
(17) Garcia, P. M. P.; Di Franco, T.; Orsino, A.; Ren, P.; Hu, X. L. *Org. Lett.* **2012**, *14*, 4286-4289.
(18) Breitenfeld, J.; Vechorkin, O.; Corminboeuf, C.; Scopelliti, R.; Hu, X. L. *Organometallics* **2010**, *29*, 3686-3689.
(19) Breitenfeld, J.; Scopelliti, R.; Hu, X. L. *Organometallics* **2012**, *31*, 2128-2136.
(20) Breitenfeld, J.; Ruiz, J.; Wodrich, M. D.; Hu, X. L. *J. Am. Chem. Soc.* **2013**, *135*, 12004-12012.
(21) Biswas, S.; Weix, D. J. *J. Am. Chem. Soc.* **2013**, *135*, 16192-16197.
(22) Zheng, B.; Tang , F. Z.; Luo , J.; Schultz , J. S.; Rath, N. P.; Mirica, L. M. *J. Am. Chem. Soc.* **2014**, *136*, 6499-6504.
(23) Lipschutz, M. I.; Tilley, T. D. *Angew. Chem., Int. Ed.* **2014**, doi: 10.1002/anie.201404577.
(24) Di Franco, T.; Boutin, N.; Hu, X. L. *Synthesis* **2013**, *45*, 2949-2958.
(25) Daikh, B. E.; Finke, R. G. *J. Am. Chem. Soc.* **1991**, *113*, 4160-4172.
(26) Poli, R. *Angew. Chem., Int. Ed.* **2006**, *45*, 5058-5070.
(27) Morrell, D. G.; Kochi, J. K. *J. Am. Chem. Soc.* **1975**, *97*, 7262-7270.
(28) Kinney, R. J.; Jones, W. D.; Bergman, R. G. *J. Am. Chem. Soc.* **1978**, *100*, 635-637.
(29) Kinney, R. J.; Jones, W. D.; Bergman, R. G. *J. Am. Chem. Soc.* **1978**, *100*, 7902-7915.
(30) Fossey, J. S.; Lefort, D.; Sorba, J. *Free radicals in organic chemistry*; Wiley, 1995.
(31) Griller, D.; Ingold, K. U. *Acc. Chem. Res.* **1980**, *13*, 317-323.
(32) Frisch, M. J.; Trucks, G. W.; Schlegel, H. B.; Scuseria, G. E.; Robb, M. A.; Cheeseman, J. R.; Scalmani, G.; Barone, V.; Mennucci, B.; Petersson, G. A.;

Nakatsuji, H.; Caricato, M.; Li, X.; Hratchian, H. P.; Izmaylov, A. F.; Bloino, J.; Zheng, G.; Sonnenberg, J. L.; Hada, M.; Ehara, M.; Toyota, K.; Fukuda, R.; Hasegawa, J.; Ishida, M.; Nakajima, T.; Honda, Y.; Kitao, O.; Nakai, H.; Vreven, T.; Montgomery, J., J. A.; Peralta, J. E.; Ogliaro, F.; Bearpark, M.; Heyd, J. J.; Brothers, E.; Kudin, K. N.; Staroverov, V. N.; Kobayashi, R.; Normand, J.; Raghavachari, K.; Rendell, A.; Burant, J. C.; Iyengar, S. S.; Tomasi, J.; Cossi, M.; Rega, N.; Millam, M. J.; Klene, M.; Knox, J. E.; Cross, J. B.; Bakken, V.; Adamo, C.; Jaramillo, J.; Gomperts, R.; Stratmann, R. E.; Yazyev, O.; Austin, A. J.; Cammi, R.; Pomelli, C.; Ochterski, J. W.; Martin, R. L.; Morokuma, K.; Zakrzewski, V. G.; Voth, G. A.; Salvador, P.; Dannenberg, J. J.; Dapprich, S.; Daniels, A. D.; Farkas, O.; Foresman, J. B.; Ortiz, J. V.; Cioslowski, J.; Fox, D. J.; Gaussian, Inc.: Wallingford, CT, 2009.
(33) Schafer, A.; Horn, H.; Ahlrichs, R. *J. Chem. Phys.* **1992**, *97*, 2571-2577.
(34) Zhao, Y.; Truhlar, D. G. *Acc. Chem. Res.* **2008**, *41*, 157-167.
(35) Zhao, Y.; Truhlar, D. G. *Theor. Chem. Acc.* **2008**, *120*, 215-241.
(36) Perdew, J. P.; Burke, K.; Ernzerhof, M. *Phys. Rev. Lett.* **1996**, *77*, 3865-3868.
(37) Adamo, C.; Barone, V. *J. Chem. Phys.* **1999**, *110*, 6158-6170.
(38) Steinmann, S. N.; Corminboeuf, C. *J. Chem. Theory Comput.* **2010**, *6*, 1990-2001.
(39) Steinmann, S. N.; Corminboeuf, C. *Chimia* **2011**, *65*, 240-244.
(40) Steinmann, S. N.; Corminboeuf, C. *J. Chem. Phys.* **2011**, *134*, 044117.
(41) Steinmann, S. N.; Corminboeuf, C. *J. Chem. Theory Comput.* **2011**, 3567-3577.
(42) te Velde, G.; Bickelhaupt, F. M.; van Gisbergen, S. J. A.; Fonseca Guerra, C.; Baerends, E. J.; Snijders, J. G.; Ziegler, T. *J. Comput. Chem.* **2001**, *22*, 931-967.
(43) Fonseca Guerra, C.; Snijders, J. G.; te Velde, G.; Baerends, E. J. *Theor. Chem. Acc.* **1998**, *99*, 391-403.
(44) Klamt, A. *WIREs Comp. Mol. Sci.* **2011**, *1*, 699-709.
(45) Adhikari, D.; Mossin, S.; Basuli, F.; Huffman, J. C.; Szilagyi, R. K.; Meyer, K.; Mindiola, D. J. *J. Am. Chem. Soc.* **2008**, *130*, 3676-3682.
(46) Suarez, A. I. O.; Lyaskovskyy, V.; Reek, J. N. H.; van der Vlugt, J. I.; de Bruin, B. *Angew. Chem., Int. Ed.* **2013**, *52*, 12510-12529.
(47) Yamamoto, T.; Wakabayashi, S.; Osakada, K. *J. Organomet. Chem.* **1992**, *428*, 223-237.
(48) Osakada, K.; Yamamoto, T. *Coord. Chem. Rev.* **2000**, *198*, 379-399.
(49) Ren, P.; Vechorkin, O.; Csok, Z.; Salihu, I.; Scopelliti, R.; Hu, X. L. *Dalton Trans.* **2011**, *40*, 8906-8911.
(50) Love, B. E.; Jones, E. G. *J. Org. Chem.* **1999**, *64*, 3755-3756.
(51) Graham, T. J. A.; Poole, T. H.; Reese, C. N.; Goess, B. C. *J. Org. Chem.* **2011**, *76*, 4132-4138.
(52) Ahmadjunan, S. A.; Walkington, A. J.; Whiting, D. A. *J. Chem. Soc.-Perkin Trans. 1* **1992**, 2313-2320.
(53) Yato, M.; Homma, K.; Ishida, A. *Tetrahedron* **2001**, *57*, 5353-5359.